

Comparative study of the thermal stability of Be-based extreme ultraviolet pellicles

© S.Yu. Zuev, A.Ya. Lopatin, V.I. Luchin, N.N. Salashchenko, D.A. Tatarskiy, N.N. Tsybin, N.I. Chkhalo

Institute of Physics of Microstructures, Russian Academy of Sciences, Nizhny Novgorod, Russia
e-mail: tsybin@ipmras.ru

Received June 28, 2021

Revised August 26, 2021

Accepted August 31, 2021

We demonstrate the possibility of manufacturing Be-based ultrathin films with high transmission at wavelengths of 11.4 and 13.5 nm. For free-standing films of Be and Be-based multilayer structures (Si/Be, ZrSi₂/Be, Be/BexNy, Zr/Be, Ru/Be, Mo/Be), we determine the thresholds of the absorbed power at which over a short period (tens of minutes) of vacuum annealing, initially sagging free-standing films became visibly stretched over the hole. Of the film structures tested here, the Be/BexNy structure (with beryllium nitride interlayers) showed the highest threshold for the absorbed power (1 W/cm²). However, due to the low strength of this structure, ZrSi₂/Be, Mo/Be, and Be films seem to be more promising for the manufacture of a full-size pellicle. Long-term vacuum annealing of Mo/Be and Be ultrathin films showed that they could withstand 24 hours of vacuum heating at an absorbed power density of 0.2 W/cm² (film temperature 250°C) without noticeable changes in EUV transmission or sagging of films. With comparable transmission (~83% at 13.5 nm and ~88% at 11.4 nm), a multilayer Mo/Be structure with a thickness of 30 nm appears to be preferable, as it shows less brittleness than a monolayer Be film with a thickness of 50 nm.

Keywords: Be-based pellicle, multilayer thin film, EUV lithography, thermal stability

DOI: 10.21883/TP.2022.01.52535.197-21

Introduction

Silicon-containing free-standing films are used in scanners for extreme ultraviolet (EUV) lithography (at a wavelength of 13.5 nm) as a protective screen (pellicle) shielding the photographic mask from dust particles and other contaminants [1,2] and as a membrane (DGL filter) separating the vacuum chamber with projection optics from the working volume (where the EUV resist is exposed) and preventing the deposition of products of resist outgassing on the surface of optical elements [3,4]. These films may also serve additionally as spectral filters suppressing unwanted out-of-band emission in the spectrum of a laser plasma source (e.g., emission in the wavelength range of 100–400 nm to which the EUV resist is sensitive) [4].

A pellicle prevents the deposition of contaminants on the mask surface. Dust particles deposited on the surface of a pellicle, which is located at a distance of several millimeters from the mask, are out of focus and, being less than 10 μm in size, do not exert a significant effect on the image formed in the EUV resist [1].

Used as protective screens and membranes in EUV scanners, films should not distort and attenuate substantially the transmitted EUV radiation in the working wavelength range. The materials most transparent at the working wavelength are thus chosen for pellicles and DGL filters, and the films themselves are made to be as thin as possible. The typical thickness range of pellicles is 35–50 nm. It is limited from below both by the strength of materials and, in part, by the fabrication techniques.

The complexity of fabrication of pellicles with a large aperture exceeding the mask size (104 × 132 mm) is compounded by another problem related to local heating of the film in the exposed region. In an effort to enhance the performance of EUV scanners, engineers increase the power of laser plasma sources of EUV radiation. The power of EUV radiation focused by the collector mirror (at the intermediate focus) near the working wavelength of 13.5 nm has already reached 250 W in newer machines [5,6]. A pellicle is then irradiated with an EUV radiation power density of about 5 W/cm². Approximately 1 W/cm² from this power density is absorbed in a double pass (for a pellicle with a transmission coefficient of 90% at a wavelength of 13.5 nm in a single pass), inducing local pellicle heating to temperatures in excess of 500°C [7]. High temperatures accelerate the processes of oxidation of the film material and induce the deposition of carbon contaminants from carbon gases, which are present in the scanner atmosphere, on films, thus reducing the transmission coefficient of film elements in the EUV wavelength range. Local heating of films may also lead to their disruption due to internal stress caused by the structural changes (e.g., as a result of crystallization of the initially amorphous film material). In addition, since the exposed region moves along a pellicle (due to the movement of the mask together with the pellicle in the process of scanning), the film temperature in the region of exposure varies cyclically from the minimum (room temperature) to the maximum one. In due time, this may result in fatigue rupture of the pellicle material.

Laser plasma sources of EUV radiation generating more than 300 W at the intermediate focus [8–10] are already being tested at research laboratories. In order to use such radiation sources in scanners, one needs to fabricate film structures with their thermal stability exceeding that of the currently available films.

It should be noted that the thermal load on a pellicle is specified by the balance between heating, which is induced by the absorption of radiation transmitted twice (since a reflective mask is used in the EUV range) through the film, and cooling, which is governed by thermal radiation (other cooling methods are less efficient for a pellicle).

Since no material is fully transparent in the EUV wavelength range, materials with the lowest possible absorption coefficient are chosen for pellicles. One such material suitable for a wavelength of 13.5 nm is silicon. However, a thin uniform film of polycrystalline silicon (*p*-Si) cannot withstand high thermal loads and may be damaged under a load equivalent to exposure to a radiation source with a power of 80 W at the intermediate focus [11,12]. The film damage is caused by high temperatures due to inefficient cooling, since the infrared (IR) emissivity of a *p*-Si pellicle 50 nm in thickness is low (approximately 0.02 at room temperature). The characteristics of *p*-Si pellicles are enhanced by coating them with thin layers of materials with high IR emissivity values. Specifically, nanometer-thick ruthenium coatings deposited on either side of a silicon film raise its IR emissivity up to 0.2–0.4, which is close to the emissivity of a Ru layer 2–3 nm in thickness [13,14]. Although coatings raise the absorption of EUV radiation, this IR emissivity enhancement provides an opportunity to reduce the film temperature considerably. Thus, *p*-Si pellicles and DGL filters with nanometer coatings are used efficiently in scanners with an EUV radiation source with a power of 250 W at the intermediate focus.

However, since film structures made from polycrystalline silicon work at the limit of their thermal stability in state-of-the-art EUV scanners [12,15], new materials for pellicles are being researched actively around the globe. These new materials should satisfy all the process requirements and at the same time be able to withstand high thermal loads in EUV scanners with laser plasma radiation source, the power of which exceeds 250 W at the intermediate focus. The following possible materials are studied extensively: silicides of metals that are relatively transparent at a wavelength of 13.5 nm [7] (including nitrided metal silicides [16]), silicon nitride [13], and graphite [17,18]. Porous films of carbon nanotubes may also be used as pellicles [19].

Each of these options has its drawbacks. Although carbon-based films have high thermal stability and high emissivity (e.g., it was demonstrated in [20] that films made from carbon nanotubes withstand short-duration heating with a thermal load equivalent to that of a pellicle exposed to EUV radiation from a source with a power of 600 W at the intermediate focus), film structures based on carbon degrade in the process of heating in the scanner atmosphere that contains hydrogen [21]. Since films made from metal

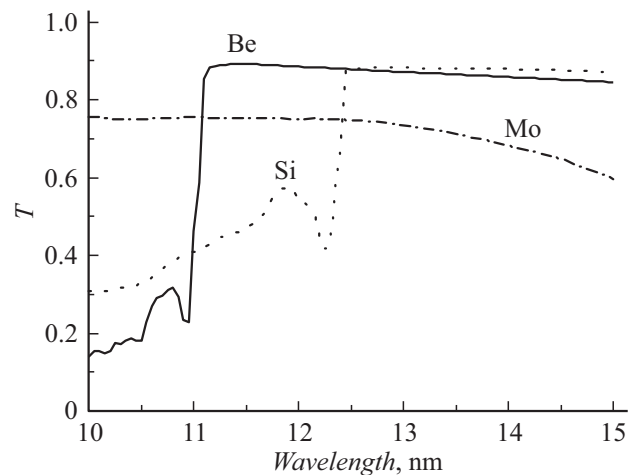


Figure 1. Transmission spectra of Be, Si, and Mo films 50 nm in thickness calculated based on the optical constants taken from [24]. It was assumed in calculations that the surfaces of films have natural oxide coating layers with a thickness of 2.5 nm.

silicides (ZrSi_2 , MoSi_2) withstand thermal loads comparable to those withstood by *p*-Si films [22], they have no obvious advantages, while films made from nitrided zirconium and molybdenum silicides are more thermally stable than *p*-Si films (including those with nanometer coatings), but are less transparent [16]. Silicon nitride films are more thermally stable than *p*-Si films. However, the IR emissivity of silicon nitride is even lower than that of polycrystalline silicon, and SiN_x pellicles (54 nm in thickness) without coatings withstand approximately the same thermal loads (less than 80 W of equivalent power at the intermediate focus [23]) as *p*-Si pellicles.

The ways to mitigate these disadvantages of film structures and new materials for pellicles are now being researched actively.

In the present study, we examine beryllium-based pellicles with a focus on their thermal stability. Beryllium was chosen due to the fact that it ranks (alongside with silicon) among the most transparent materials at a wavelength of 13.5 nm (Fig. 1).

1. Research methods

A special laboratory for experiments with beryllium has been outfitted at the Institute for Physics of Microstructures of the Russian Academy of Sciences. It features ventilation and exhaust systems with several filtration stages and satisfies all safety standards. A four-magnetron sputtering setup was used to fabricate film samples [25]. The sputtering of targets was performed in argon environment (in the case of interlayers of nitrided beryllium Be_xN_y , a mixture of N_2 and Ar gases with ratio of partial pressures $p_{\text{N}_2}/p_{\text{Ar}} = 1/5$ was used) at a pressure of $7 \cdot 10^{-4}$ Torr. The residual pressure in the vacuum chamber prior to sputtering was below 10^{-6} Torr.

The ratio of partial pressures of nitrogen and argon in the process of deposition of Be_xN_y layers was set to be rather large (see, for example, earlier study [16] on films made from nitrided zirconium and molybdenum silicides) to ensure a high concentration of nitrogen in layers. The exact nitrogen and beryllium content of nitrided beryllium layers was not determined. It is plausible to assume that the fraction of nitrogen is close to (or somewhat lower than) that in Be_3N_2 .

Free-standing Be-containing films were fabricated using an Mg sacrificial layer and a selective etchant (aqueous solution of acetic acid); see [25] for details. The thicknesses of the film layers in multilayer compositions were determined using data from grazing incidence reflectometry obtained with a Panalytical X'Pert Pro diffractometer (wavelength $\lambda = 0.154$ nm).

The films were heated in vacuum (the residual pressure was $\sim 10^{-8}$ Torr with evacuation during annealing performed by an NMD-0.4 getter-ion pump) by passing current through a free-standing film. The test stand [26] allowed for hours-long annealing with the power released in the film kept constant. Be-containing films were attached to quartz frames with contact pads formed on them. Quartz frames had a square through aperture 8×8 mm in size at the center. Electrical current was passed through films via vacuum input leads and pressure contacts. The films were thus heated due to the release of Joule heat. The use of a four-contact arrangement and controllers provided an opportunity to maintain automatically a constant power release in free-standing films of different composition throughout the entire process.

The film could be monitored visually through inspection windows in the vacuum chamber.

A Metis MB35 infrared pyrometer (operating wavelength range: $2\text{--}5\ \mu\text{m}$) was used to measure the film temperature at the center of the aperture through a CaF_2 window. The IR pyrometer readings depended on the preset value of emissivity ε . The method used to determine ε for relatively thick film samples at a temperature of $130\text{--}150^\circ\text{C}$ was detailed in [22,26].

However, this method is not suitable for the determination of emissivity of ultrathin films that become transparent for IR radiation. In addition, since the emissivity of uniform films varies considerably with thickness [27] and becomes more and more dependent on the state of surface layers (the presence of oxides and carbon contaminants) as films get thinner, it is incorrect to use the values of emissivity determined for thicker films in the measurement of temperature of ultrathin films of the same composition.

That said, the IR pyrometer readings for ultrathin films (rough estimates of the temperature of a free-standing film at the center of the aperture) are provided in the text for guidance. These data were obtained on the assumption that the studied ultrathin films have equal values of emissivity $\varepsilon = 0.2$, which is close to the value measured for a multilayer Mo/Be structure with a thickness of 50 nm.

One should bear in mind that the film temperature is not significant in comparative tests of materials for pellicles; the relevant value is the maximum absorbed power density withstood by an ultrathin film in the process of heating without changes in its properties.

A laboratory reflectometer with an RSM-500 spectrometer/monochromator and an X-ray tube radiation source was used to measure the EUV transmission coefficients of ultrathin films before and after vacuum annealing [28].

Several film samples were compared in their ultimate rupture strength. Films were mounted on silicon frames with a circular aperture 2.5 mm in diameter. A pressure drop between the sides of a film was induced, and the limit drop at which the film got disrupted was measured.

2. Preliminary tests. Short-term annealing

One significant drawback of beryllium is its brittleness [29]. The use of multilayer structures with brittle Be layers interleaved with layers made from other materials (preferably those having higher plasticity) is one of the possible ways of mitigating this drawback [30]. Multilayer compositions can also have greater strength [31].

Note that, in certain cases, the mechanical properties of free-standing films may be enhanced by thin coatings deposited on either side. This was observed, e.g., for Al film structures with nanometer MoSi_2 protective coatings on either side [26]. Our attempt to enhance the strength of a Be film in this way was rather fruitless (Table 1). In addition, since crystallization of initially amorphous cap layers (such as MoSi_2) can in principle contribute to the tension of the film upon heating we did not examine three-layer compositions in the present study and focused on multilayer periodic Be-containing structures without protective coatings.

The following materials relatively transparent at 13.5 nm were chosen to be paired up with beryllium in multilayer compositions: Si, Zr, ZrSi_2 , Mo, Ru. A multilayer film with beryllium interleaved with nitrided beryllium layers (Be_xN_y) was also examined on the assumption that

Table 1. Limit pressure drops Δp (averaged over 8–12 trials) between the sides of a film at which the film got disrupted

Structure, nm	Film thickness, nm	Δp_{mean} , atm	σ , atm
Al-150	150	0.057	0.03
$\text{MoSi}_2\text{-}2.5, \text{Al-}150, \text{MoSi}_2\text{-}2.5$	155	0.18	0.07
Be-150	150	0.092	0.067
$\text{MoSi}_2\text{-}3, \text{Be-}150, \text{MoSi}_2\text{-}3$	156	0.102	0.088

Note: the diameter of the aperture in the silicon frame is 2.5 mm; σ is the root-mean-square deviation.

Table 2. Absorbed power density (q) at which Be-containing free-standing films secured along the perimeter of the frame aperture become visibly stretched during short-term (15–30 min) annealing in vacuum

Structure (thickness in nm)	q , W/cm ²	ε	T , °C
(Si-2.5/Be-1.5)×15	0.1	0.34	165–170
(ZrSi ₂ -2/Be-2.5)×23	0.4	0.3	~ 330
(Be-2.5/Be _x N _y -2.5)×20	1	–	~ 530 at $\varepsilon = 0.2$
(Zr-2.5/Be-2.5)×40	0.15	–	~ 255 at $\varepsilon = 0.2$
(Ru-2/Be-2.5)×10	0.2	0.2	~ 260
(Mo-2/Be-2)×10	0.4	0.18	~ 360
Be-160	0.5	0.14	~ 495

Note: ε is the emissivity determined at temperatures of 130–150°C; T is the film temperature at the center of the aperture measured with the IR pyrometer.

beryllium nitride may be more resistant to oxidation than beryllium [32].

Since the number of possible versions of multilayer structures based on Be is rather large, we split the study into two stages. At the first stage, the aim was to choose such structures that withstand short-term vacuum heating at the highest absorbed power densities. Relatively thick (up to 200 nm) samples of free-standing films were used in these preliminary experiments. Such samples are easier to manufacture and handle.

The experiment was conducted in accordance with the following procedure. The examined film structure on a quartz frame was introduced into a vacuum chamber. Owing to the specifics of the fabrication process, the as-prepared film was sagging over the aperture (formed wrinkles). In the process of heating in vacuum, the power density applied to the film increased gradually (with a pitch of 0.05 W/cm²), and the state of the free-standing part of the film was monitored through the vacuum chamber window. The threshold level (q) was assumed to correspond to the absorbed power density at which the film became visibly stretched over the aperture (i.e., the free-standing film sagging over the aperture became mirror-like) in a short period of time (15–30 min).

The results of monitoring of films of different composition subjected to vacuum annealing provided an opportunity to compare roughly their resistances to thermal loads (with regard only to the changes in structural properties; the changes in optical properties were neglected). The results of such tests of Be-containing films are presented in Table 2.

It follows from Table 2 that films of different composition become stretched over the aperture at significantly different values of absorbed power density q and temperature. The reasons for this spread are not entirely clear.

The stretching of a beryllium film over the aperture in the process of heating is apparently associated with an increase in the fraction of the crystalline phase (emergence and growth of crystallites), which is accompanied by a reduction in the specific volume of the film and, consequently, stretching of the free-standing film secured along the perimeter of the aperture. Figure 2 shows a 160-nm Be film (as-prepared (Fig. 2, *a*) and annealed at an absorbed power density of 0.55 W/cm² for 2.5 h (Fig. 2, *b*)) imaged with a LIBRA 200MC transmission electron microscope. It can be seen that crystallites increase in size after annealing.

In the case of ZrSi₂/Be and Si/Be structures, film stretching may be related to the crystallization of initially amorphous ZrSi₂ and Si layers. For example, as was shown earlier in [16], a single-layer ZrSi₂ film subjected to vacuum annealing becomes stretched promptly (within several minutes) over the aperture when the absorbed power density increases to 0.5 W/cm² (the film temperature is ~ 325°C, $\varepsilon = 0.35$).

As for multilayer structures with Be layers interleaved with other metals, it is still unclear why free-standing films of this kind become stretched at significantly lower temperatures than uniform multilayer structures (take, for example, Ru/Be structures: the stretching of separate Be and Ru free-standing films subjected to short-term vacuum annealing was not observed at temperatures below 500°C). This issue requires further study. The same is true for the substantial difference between the threshold power density values for Mo/Be and Zr/Be, Ru/Be multilayer structures that have close values of emissivity.

As for the Be/Be_xN_y structure, it is reasonable to assume that the presence of nitrogen in interlayers inhibits their crystallization on heating, while the amorphous Be_xN_y interlayers themselves may hinder the growth of crystallites in beryllium layers (at least in the direction perpendicular to the layer plane). Apparently, these factors and the relatively high emissivity are the reasons why Be/Be_xN_y demonstrated the highest resistance to thermal loads among all the tested structures.

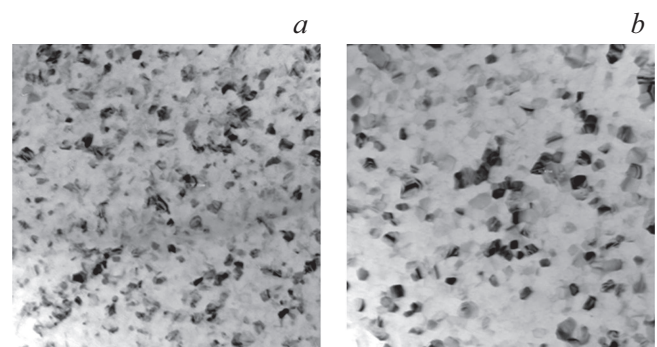


Figure 2. TEM image of a Be film with a thickness of 160 nm prior to (*a*) and after (*b*) vacuum annealing at $q = 0.55$ W/cm² (temperature of the film is ~ 515°C, $\varepsilon = 0.14$) for 2.5 h. The frames are approximately 900 nm in size.

3. Comparison of thermal stability of ultrathin Be, Mo/Be, and ZrSi₂/Be films

Although the Be/Be_xN_y multilayer structure was the best of all the examined Be-containing films in preliminary tests, it was excluded from the second test stage due to its insufficient strength. A Be/Be_xN_y film turned out to be even less durable than a uniform beryllium film of a comparable thickness. In addition, it was found that nitrided beryllium layers are less chemically stable than beryllium layers and are dissolved in the selective etchant. This causes gradual dissolution of the Be/Be_xN_y film in the process of its separation from the substrate, but does not preclude one from fabricating small-sized samples if beryllium layers are the outer ones. Evidently, these specifics of material properties may hinder the fabrication of large-aperture Be/Be_xN_y ultrathin films.

Three structures (Be, Mo/Be, ZrSi₂/Be) were chosen based on the results of preliminary tests. Their stretching was observed at relatively high absorbed power densities, and their strength and plasticity were sufficient to fabricate free-standing films that are highly transparent in the operating range.

Free-standing films of the following compositions were subjected to comparative tests: Be films 50 nm in thickness and multilayer Be-2,(Mo-2/Be-2)×7 and Be-2,(ZrSi₂-2/Be-2)×7 structures (the thickness is given in nanometers). The indicated film structures were subjected to vacuum heating at equal power densities (first at 0.3 W/cm², and then at smaller loads) for 24 h. The transmission coefficients of films were measured at wavelengths $\lambda = 11.4$ and 13.5 nm before and after heating.

In all three cases, the free-standing part of films became visibly stretched after several hours of annealing at an absorbed power density of 0.3 W/cm² (the corresponding temperature at the center of films is 300–320°C if emissivity ε is assumed to be equal to 0.2). They became overstretched as heating was being terminated (at a constant rate within several tens of minutes) after 24 h. Cracks formed as a result (Fig. 3).

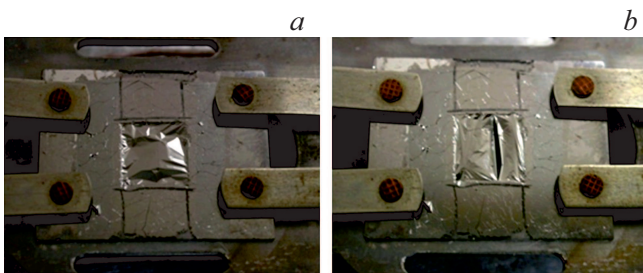


Figure 3. Photographic images of an ultrathin Be film on a quartz frame with a square aperture 8×8 mm in size before (a) and after (b) annealing at 0.3 W/cm² for 24 h. It is seen clearly that a crack in the film formed when heating was terminated (b).

Table 3. Transmission coefficients of ultrathin films ($\lambda = 13.5$ nm) before ($T_{initial}$) and after (T_{anneal}) 24 h of annealing at 0.3 W/cm²

Films	Be (50 nm)	Mo/Be (30 nm)	ZrSi ₂ /Be (30 nm)
$T_{initial}$	0.827	0.823	0.873
T_{anneal}	0.805	0.804	0.844

Table 4. Transmission coefficients of ultrathin films ($\lambda = 11.4$ nm) before ($T_{initial}$) and after (T_{anneal}) 24 h of annealing at 0.3 W/cm²

Films	Be (50 nm)	Mo/Be (30 nm)	ZrSi ₂ /Be (30 nm)
$T_{initial}$	0.880	0.874	0.793
T_{anneal}	0.866	0.864	0.773

The transmission coefficients of film samples at 11.4 and 13.5 nm (see Tables 3 and 4) decreased somewhat after annealing. This was apparently caused by the oxidation of outer Be layers and, probably, the material of deeper layers. It is fair to assume that an enhanced resistance of Mo layers to oxidation is the reason why the change in transmission coefficients for the Mo/Be structure is less significant than the change for Be and ZrSi₂/Be.

After 24 h of vacuum annealing at 0.2 W/cm² (the corresponding film temperature at the aperture center is $\sim 250^\circ\text{C}$ if ε is assumed to be equal to 0.2), the free-standing part of the film became stretched only for ZrSi₂/Be and only at the stage of termination of heating. The external appearance of Be and Mo/Be film samples remained unchanged after 24 h of annealing. The transmission coefficient at 11.4 and 13.5 nm remained unchanged (within 1% in absolute values; i.e., within the accuracy of measurements) for all three types of pellicles. Note that the value of 0.2 W/cm² is significantly lower than the values of q determined for these structures in preliminary tests. This is attributable to the fact that the heating time was longer (and, possibly, to the variation of IR emissivity with thickness of films).

The absorbed power density of 0.2 W/cm² is roughly equivalent to the thermal load on a pellicle provided by an EUV source generating 40 W at the intermediate focus. Thus, the capacity of Be and Mo/Be ultrathin film structures to withstand thermal loads was comparable to (or slightly lower than) that of Si and SiN_x ultrathin films. Although the Mo/Be structure is substantially thinner than Be films, it turned out to be more durable. This is evidenced by the average values of pressure drop at which films become disrupted: $\Delta p = 0.18$ atm for a Be-2,(Mo-2/Be-2)×22 film with a thickness of 90 nm and $\Delta p = 0.092$ atm for a Be film with a thickness of 150 nm over apertures 2.5 mm in diameter.

Conclusion

Since beryllium is transparent at wavelengths beyond the K absorption edge ($\lambda \geq 11.1$ nm), it is a promising material for fabrication of highly transparent film elements for projection lithography units operating at a wavelength of 13.5 nm. In the present study, several configurations of pellicles based on beryllium were considered. The absorbed power density thresholds (i.e., the levels that such film structures have the capacity to withstand when subjected to 24 h of vacuum heating) were determined for the best candidate structures.

The examination of influence of short-term (15–30 min) vacuum heating on the stretching of free-standing Be, Si/Be, ZrSi₂/Be, Be/Be_xN_y, Zr/Be, Ru/Be, and Mo/Be films revealed that the free-standing part of the Be/Be_xN_y film becomes visibly stretched over the aperture after 20 min of annealing at an absorbed power of approximately 1 W/cm², which corresponds to the pellicle exposure to an EUV radiation source with a power of 250 W at the intermediate focus. This is the highest result among all the tested Be-containing film structures. Presumably, the thermal stability of Be/Be_xN_y comes from the fact that nitrogen prevents the crystallization of initially amorphous Be_xN_y layers during heating, while Be_xN_y interlayers, in turn, prevent the growth of crystallites in polycrystalline beryllium layers. However, the Be/Be_xN_y film structure turned out to be less chemically stable (Be_xN_y layers dissolved on contact with an acetic acid solution in the process of separation of films from substrates) and less durable than a uniform beryllium film of a comparable thickness. This may hinder the fabrication of full-size pellicles of this composition. Our future studies will be aimed at enhancing the strength of this film structure and finding a new solvent that does not interact with Be_xN_y.

Multilayer ZrSi₂/Be and Mo/Be films and single-layer Be films were fairly resistant to short-term heating and more durable than the Be/Be_xN_y film structure. Ultrathin free-standing Be, ZrSi₂/Be and Mo/Be films were heated in vacuum for 24 h at different thermal loads. ZrSi₂/Be films (30 nm in thickness) were less thermally stable than Be and Mo/Be films (free-standing ZrSi₂/Be films became stretched over the aperture when heating was terminated after 24 h of annealing at 0.2 W/cm²). The thermal stability of Be films (50 nm in thickness) was comparable to that of Mo/Be films (30 nm in thickness): both structures withstood 24 h of heating in vacuum at an absorbed power density of 0.2 W/cm². Free-standing Be and Mo/Be films remained sagging after tests, and their EUV transmission coefficient remained unchanged within the accuracy of measurements (1% in absolute values). Thus, one may conclude that Be and Mo/Be pellicles have the capacity to withstand thermal loads equivalent to the exposure to an EUV radiation source with a power of 40 W in a scanner. Therefore, the capacity of ultrathin Be and Mo/Be films to retain their properties under thermal loads in an EUV scanner is comparable to (or just slightly lower than) that of ultrathin p -Si and SiN_x films.

Funding

The work was performed under the state assignment of the Institute for Physics of Microstructures of the Russian Academy of Sciences (No. 0030-2021-0022) and was supported by grants from the Russian Foundation for Basic Research (projects Nos. 19-07-00173 and 19-02-00081). Equipment of the Physics and Technology of Micro- and Nanostructures common research center was used.

Conflict of interest

The authors declare that they have no conflict of interest.

References

- [1] L. Scaccabarozzi, D. Smith, P.R. Diago, E. Casimiri, N. Dziomkina, H. Meijer. *Proc. SPIE*, **8679**, 867904 (2013). DOI: 10.1117/12.2015833
- [2] Y. Hyun, J. Kim, K. Kim, S. Koo, S. Kim, Y. Kim, C. Lim, N. Kwak. *Proc. SPIE*, **9422**, 94221U (2015). DOI: 10.1117/12.2085626
- [3] M. van de Kerkhof, H. Jasper, L. Levasier, R. Peeters, R. van Es, J.-W. Bosker, A. Zdravkov, E. Lenderink, F. Evangelista, P. Broman, B. Bilski, T. Last. *Proc. SPIE*, **10143**, 101430D (2017). DOI: 10.1117/12.2258025
- [4] M.A. van de Kerkhof, F. Liu, M. Meeuwissen, X. Zhang, M. Bayraktar, R.C. de Kruijf, N.V. Davydova. *J. Micro-Nanolith. MEM.*, **19** (3), 033801 (2020). DOI: 10.1117/1.JMM.19.3.033801
- [5] N. Fu, Y. Liu, X. Ma, Z. Chen. *J. Microelectron. Manuf.*, **2**, 19020202 (2019). DOI: 10.33079/jomm.19020202
- [6] R. van Es, M. van de Kerkhof, A. Minnaert, G. Fisser, J. de Klerk, J. Smits, R. Moors, E. Verhoeven, L. Levasier, R. Peeters, M. Pieters, H. Meiling. *Proc. SPIE*, **10583**, 105830H (2018). DOI: 10.1117/12.2299503
- [7] P.J. van Zwol, M. Nasalevich, W.P. Voorthuijzen, E. Kurganova, A. Notenboom, D. Vles, M. Peter, W. Symens, A.J.M. Giesbers, J.H. Klootwijk, R.W.E. van de Kruijs, W.J. van der Zande. *Proc. SPIE*, **10451**, 104510O (2017). DOI: 10.1117/12.2280560
- [8] H. Mizoguchi, H. Nakarai, T. Abe, H. Tanaka, Yu. Watanabe, T. Hori, Yu. Shiraishi, T. Yanagida, G. Soumagne, T. Yamada, T. Saitou. *Proc. SPIE*, **11323**, 113230X (2020). DOI: 10.1117/12.2549905
- [9] D.C. Brandt, M. Purvis, I. Fomenkov, D. Brown, A. Schafgans, P. Mayer, R. Rafac. *Proc. SPIE*, **11609**, 116091E (2021). DOI: 10.1117/12.2584413
- [10] H. Mizoguchi, H. Nakarai, T. Abe, H. Tanaka, Yu. Watanabe, T. Hori, Yu. Shiraishi, T. Yanagida, G. Sumangne, T. Yamada, T. Saitou. *Proc. SPIE*, **11609**, 1160919 (2021). DOI: 10.1117/12.2581910
- [11] J. Wiley. *EUV Pellicle Progress and Strategy. iEUVi Mask TWG Meeting* (Toyama, Japan, 2013)
- [12] C. Zoldesi, K. Bal, B. Blum, G. Bock, D. Brouns, F. Dhalluin, N. Dziomkina, J.D.A. Espinoza, J. de Hoogh, S. Houweling, M. Jansen, M. Kamali, A. Kempa, R. Kox, R. de Kruijf, J. Lima, Y. Liu, H. Meijer, H. Meiling, I. van Mil, M. Reijnen, L. Scaccabarozzi, D. Smith, B. Verbrugge, L. de Winters, X. Xiong, J. Zimmerman. *A. Proc. SPIE*, **9048**, 90481N (2014). DOI: 10.1117/12.2049276

- [13] M. Nasalevich, P.J. van Zwol, E. Abegg, P. Voorthuizen, D. Vles, M. Péter, W. van der Zande, H. Vermeulen. *Proc. SPIE*, **10032**, 100320L (2016). DOI: 10.1117/12.2255040
- [14] J. Hong, C. Park, C. Lee, K. Nam, Y. Jang, S. Wi, J. Ahn. *Proc. SPIE*, **10809**, 108090R (2018). DOI: 10.1117/12.2501772
- [15] D. Brouns, P. Broman, J.-W. van der Horst, R. Lafarre, R. Maas, T. Modderman, R. Notermans, G. Salmaso. *Proc. SPIE*, **11178**, 1117806 (2019). DOI: 10.1117/12.2536344
- [16] S.Yu. Zuev, A.Ya. Lopatin, V.I. Luchin, N.N. Salashchenko, D.A. Tatarskiy, N.N. Tsybin, N.I. Chkhalo. *Tech. Phys.*, **64** (11), 1590 (2019). DOI: 10.1134/S1063784219110306
- [17] M.J. Kim, H. Chul Jeon, R. Chalykh, E. Kim, J. Na, B.-G. Kim, H. Kim, C. Jeon, S.-G. Kim, D.-W. Shin, T. Kim, S. Kim, J.H. Lee, J.-B. Yoo. *Proc. SPIE*, **9776**, 97761Z (2016). DOI: 10.1117/12.2218228
- [18] Q. Hu, S.-G. Kim, D.-W. Shin, T.-S. Kim, K.-B. Nam, M.J. Kim, H.-C. Chun, J.-B. Yoo. *Carbon*, **113**, 309 (2017). DOI: 10.1016/j.carbon.2016.11.068
- [19] M.Y. Timmermans, I. Pollentier, J.U. Lee, J. Meersschaut, O. Richard, C. Adelman, C. Huyghebaert, E.E. Gallagher. *Proc. SPIE*, **10451**, 104510P (2017). DOI: 10.1117/12.2280632
- [20] J. Bekaert, E. Gallagher, R. Jonckheere, L. Van Look, R. Aubert, V.V. Nair, M.Y. Timmermans, I. Pollentier, E. Hendrickx, A. Klein, G. Yeğen, P. Broman. *Proc. SPIE*, **11609**, 116090Z (2021). DOI: 10.1117/12.2584724
- [21] G. Zhang, P. Qi, X. Wang, Y. Lu, D. Mann, X. Li, H. Dai. *J. Am. Chem. Soc.*, **128** (18), 6026 (2006). DOI: 10.1021/ja061324b
- [22] N.I. Chkhalo, M.N. Drozdov, E.B. Kluev, A.Ya. Lopatin, V.I. Luchin, N.N. Salashchenko, N.N. Tsybin, L.A. Sjmaenok, V.E. Banine, A.M. Yakunin. *J. Micro-Nanolith. MEM.*, **11** (2), 021115 (2012). DOI: 10.1117/1.JMM.11.2.021115
- [23] Y.J. Jang, H.-J. Shin, S.J. Wi, H.N. Kim, G.S. Lee, J. Ahn. *Kor. J. Met. Mater.*, **57** (2), 124 (2019). DOI: 10.3365/KJMM.2019.57.2.124
- [24] X-Ray Interactions With Matter [Electronic source] Available at: https://henke.lbl.gov/optical_constants/
- [25] N. Chkhalo, A. Lopatin, A. Nechay, D. Pariev, A. Pestov, V. Polkovnikov, N. Salashchenko, F. Schäfers, M. Sertso, A. Sokolov, M. Svechnikov, N. Tsybin, S. Zuev. *J. Nanosci. Nanotechnol.*, **19**, 546 (2019). DOI: 10.1166/jnn.2019.16474
- [26] N.I. Chkhalo, M.N. Drozdov, S.A. Gusev, A.Ya. Lopatin, V.I. Luchin, N.N. Salashchenko, D.A. Tatarskiy, N.N. Tsybin, S.Yu. Zuev. *Appl. Opt.*, **58** (1), 21 (2019). DOI: 10.1364/AO.58.000021
- [27] P.J. van Zwol, D.F. Vles, W.P. Voorthuizen, M. Péter, H. Vermeulen, W.J. Zande, J.M. Sturm, R.W.E. van de Kruijs, F. Bijkerk. *J. Appl. Phys.*, **118**, 213107 (2015). DOI: 10.1063/1.4936851
- [28] M.S. Bibishkin, D.P. Chekhonadskih, N.I. Chkhalo, E.B. Klyuenkov, A.E. Pestov, N.N. Salashchenko, L.A. Shmaenok, I.G. Zabrodin, S.Yu. Zuev. *Proc. SPIE*, **5401**, 8-15 (2004).
- [29] A.F. Jankowski, M.A. Wall, T.G. Nieh. *J. Non-Cryst. Sol.*, **317** (1-2), 129 (2003). DOI: 10.1016/S0022-3093(02)01993-2
- [30] Q. Zhou, Y. Ren, Y. Du, D. Hua, W. Han. *Appl. Sci.*, **8** (10), 1821 (2018). DOI: 10.3390/app8101821
- [31] M.S. Bibishkin, N.I. Chkhalo, S.A. Gusev, E.B. Kluev, A.Y. Lopatin, V.I. Luchin, A.E. Pestov, N.N. Salashchenko, L.A. Shmaenok, N.N. Tsybin, S.Y. Zuev. *Proc. SPIE*, **7025**, 702502 (2008). DOI: 10.1117/12.802347
- [32] W. de la Cruz, G. Soto, F. Yubero. *Opt. Mater.*, **25** (1), 39 (2004). DOI: 10.1016/S0925-3467(03)00214-3